Journal of Materials Chemistry A

Accepted Manuscript

This is an *Accepted Manuscript*, which has been through the Royal Society of Chemistry peer review process and has been accepted for publication.

Accepted Manuscripts are published online shortly after acceptance, before technical editing, formatting and proof reading. Using this free service, authors can make their results available to the community, in citable form, before we publish the edited article. We will replace this *Accepted Manuscript* with the edited and formatted *Advance Article* as soon as it is available.

You can find more information about *Accepted Manuscripts* in the Information for Authors.

Please note that technical editing may introduce minor changes to the text and/or graphics, which may alter content. The journal's standard Terms & Conditions and the Ethical guidelines still apply. In no event shall the Royal Society of Chemistry be held responsible for any errors or omissions in this *Accepted Manuscript* or any consequences arising from the use of any information it contains.

ROYAL SOCIETY OF CHEMISTRY

www.rsc.org/materialsA

Journal of Materials Chemistry A

ARTICLE

A facile approach to alleviate photochemical degradation in high efficiency polymer solar cells

Received 00th January 20xx,
Accepted 00th January 20xx

DOI: 10.1039/x0xx00000x

www.rsc.org/

Wenchao Huang,[a] Eliot Gann,[ab] Zai-quan Xu,[ac] Lars Thomsen,[b] Yi-Bing Cheng[a]* and Christopher R. McNeill[a]*

Abstract: In this paper, it is found that residual 1,8-diiodoctane (DIO) which is used as a solvent additive in the manufacture of high-performance polymer solar cells accelerates chemical degradation of the donor polymer PBDTTT-EFT under light and air exposure especially in its blend with $PC_{71}BM$. Here we report an anti-solvent treatment which can significantly improve device stability while maintaining device efficiency over 9%. The morphological changes after anti-solvent treatment are also invesigated by a combination of synchrotron based techniques.

Introduction

Over the past decade, organic solar cells have been the subject of continuously increasing research interest. Solution processing offers a promising method for producing organic solar cells through continuous roll-to-roll processing, enabling a low manufacturing cost. Organic solar cell efficiency is continuing to increase with single junction efficiencies approaching 11% recently demonstrated.[1-7] Among the various electron donor materials employed, low bandgap, polymers based on benzo[1,2-b:4,5-b']dithiophene (BDT) have emerged as one of the most attractive electron donor families.[8-12] In particular, devices based on the polymer poly[[2,6'-4,8-di(5-ethylhexylthienyl)benzo[1,2-b;3,3-b]dithiophene]3-fluoro-2[(2-ethylhexyl)carbonyl]thieno[3,4-b]thiophenediyl (PBDTTT-EFT) (molecule structure shown in **Fig. 1 (a) and (b)**) exhibit a high efficiency of over 9% for polymer/fullerene devices and over 5% for polymer/polymer devices.[2, 5, 7, 13-15] In contrast to the significant efforts devoted to achieving high efficiencies through synthesizing new chemical structures, optimising morphology and interfacial layers,[2, 13, 16] less effort has been paid to improving the stability of high performance polymer cells which represents a major obstacle to commercialization.

The use of a high-boiling point solvent additive is a common tool employed to optimize the morphology of high performance polymer solar cells.[17-22] High performance cells based on the polymer PBDTTT-EFT are no exception where the use of the additive 1,8-diiodooctane (DIO) has been shown to improve the crystallization of polymer while inhibiting the formation of large-scale fullerene aggregates.[5, 20, 23] However, due to the low vapour pressure of the solvent additive, residual DIO remains in the blend long after spin-coating.[24] The trapped residual DIO is shown here to facilitate the degradation of PBDTTT-EFT, particularly under light and air exposure and especially in blends with the fullerene derivative $PC_{71}BM$. While DIO has not previously to our knowledge been linked with accelerated degradation of PBDTTT-EFT, degradation of similar polymers based on BDT units has been studied in previous papers.[25-28] Alem and co-workers in particular found that photo-excited BDT units react with oxygen under light illumination. Specifically, a blue shift of the main absorption peak was observed in the UV-vis spectra after only two hours of light illumination.[25] In addition, the degradation of another polymer containing the BDT unit, PTB7, both in neat films and in blends with $PC_{71}BM$ has also been probed by several different groups.[26-28] Strikingly, Soon et al. found that blends of PTB7 with $PC_{71}BM$ were less stable than neat films of PTB7, with the accelerated ageing in the blend facilitated by the generation of singlet oxygen from PTB7 triple excitons that in turn are produced via non-geminate recombination.[26] Razzell-Hollis et al. also confirmed that blends of PTB7 with $PC_{71}BM$ show a faster degradation rate than for pristine PTB7 with in-situ Raman spectroscopy.[28]

Although several approaches have demonstrated to improve device stability such as through the introduction of air-stable interfacial layers,[29, 30] understanding and improving the stability of donor materials such as PBDTTT-EFT remains largely unexplored. In this work, we demonstrate that residual DIO plays an important role in accelerating the degradation of the polymer PBDTTT-EFT in completed devices by facilitating the ingress of oxygen or/and water molecules. We furthermore demonstrate that a simple anti-solvent treatment is effective in dramatically improving the stability of PBDTTT-

[a] *Department of Materials Science and Engineering, Monash University, Wellington Road, Clayton, VIC 3800 Australia*
[b] *Australian Synchrotron, 800 Blackburn Road, Clayton, VIC 3168 Australia*
[c] *The Melbourne Centre for Nanofabrication, 151 Wellington Road, Clayton 3168, Victoria, Australia*

† Footnotes relating to the title and/or authors should appear here.
Electronic Supplementary Information (ESI) available: [details of any supplementary information available should be included here]. See DOI: 10.1039/x0xx00000x

Journal of Materials Chemistry A Accepted Manuscript

EFT:$PC_{71}BM$ solar cells through prompt removal of residual DIO from PBDTTT-EFT:$PC_{71}BM$ films, enabling the fabrication of stable devices under ambient conditions. **Fig.1 (c)** schematically depicts the anti-solvent treatment used in this study: During spin-coating of the PBDTTT-EFT:$PC_{71}BM$ blend solution, drops of the anti-solvent isopropanol (IPA) are dispensed onto the rotating substrate that induces rapid precipitation of the polymer and fullerene. Such alcohol treatment has been previously reported to improve the device performance and reproduciliby.[24, 31, 32] Here, we have found that this method facilitates removal of DIO that is important for alleviating the photochemical degradation of polymer blend. The morphological changes after anti-solvent treatment are also fully examined by a combination of synchrotron based X-rays techniques.

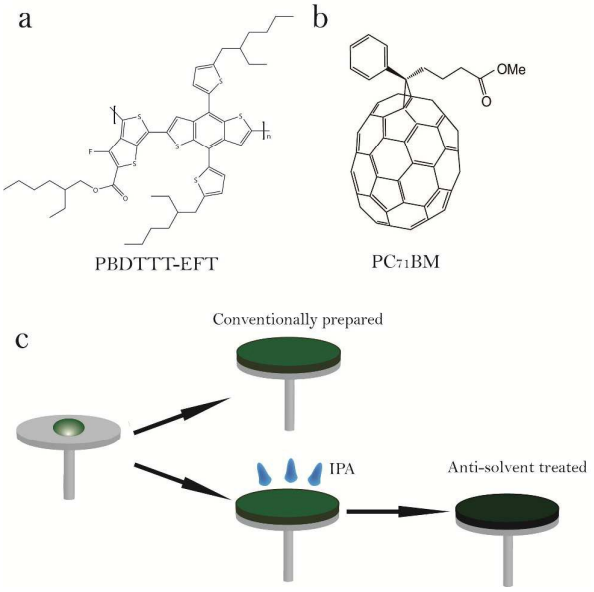

Fig.1 The molecular structure of (a) PBDTTT-EFT and (b) $PC_{71}BM$. (c) schematic of the conventional spin-coating process (top) and the anti-solvent treatment (bottom). In the anti-solvent treatment, the second solvent IPA introduced during the normal spin-coating process induces the precipitation of polymer and fullerene from the residual solvent to form a "dry film" immediately.

Methods

Materials

Polymer PBDTTT-EFT (also called PCE-10) (Mw: 114, 000, PDI: 2.2) was purchased from 1-Materials and $PC_{71}BM$ was ordered from Nano-C company. The solvent additive 1,8-diiodoctane (DIO) was purchased from Sigma Aldrich.

Device preparation

The solar cells were constructed using the inverted structure of ITO/PEIE/PBDTTT-EFT:$PC_{71}BM$/MoO3/Ag. The PEIE solution was prepared by diluting PEIE in methoxyethanol to a weight concentration of 0.4%. Indium-tin-oxide (ITO) coated glass substrates were cleaned by acetone and isopropanol respectively. The PEIE solution was spin coated on ITO/glass at the speed of 5000rpm for 30s, then sintered at 100˚C for 5 mins. On the top of PEIE, the active layer (~70nm) of PBDTTT-EFT/$PC_{71}BM$ (1:1.5, w/w) was spin-cast from solution in the co-solvent of dichlorobenzene/1, 8-diiodooctane (97:3, v/v) at a speed of 1000 rpm. For the solvent treated sample, IPA (200μL) was dropped onto the film after 120s spin-coating process. The significant colour change was observed immediately. The composite electrodes of Molybdenum oxide (15nm) and silver (100nm) were thermally deposited atop the active layer through a shadow mask with the defined area. Devices were encapsulated by the epoxy resin in the glove box.

Characterization

The current-voltage (J-V) was measured under 100mW/cm^2 by using a model SS50AAA solar simulator (Photo Emission Tech.). Devices were soaked under solar simulator for 10 mins before J-V curve measurements. The intensity of simulated sun light was calibrated by a standard silicon diode. For testing the shelf stability of the devices, polymer solar cells were stored in ambient atmosphere under the illumination of room light for up to 40 days. The external quantum efficiency (EQE) was detected by dispersing light from a tungsten filament Newport 250 W QTH) through a monochromator (Oriel Cornerstone 130) with a spot size smaller than the device active area. The short circuit current at each wavelength was recorded by using a Keithley 2635 sourcemeter.

Grazing incidence wide angle X-ray scattering (GIWAXS) was collected at the SAXS/WAXS beamline at Australian Synchrotron.[33] X-ray incident beam was monochromatic 9 KeV photons. 2D scattering patterns were collected by a Dectris Pilatus 1M with the exposure time of 1 s. This short exposure time effectively avoided X-ray induced beam damage in the samples. The GIWAXS results were analysed by an altered version of the NIKA analysis package.[34] The near edge X-ray absorption fine structure (NEXAFS) spectra at the carbon edge were measured at the soft X-ray beamline at Australian Synchrotron.[35] A surface sensitive total yield electron (TEY) was detected by the flux of the drain current. The results were analysed according to our previous study.[36-38]

Resonant soft X-ray scattering was collected at beamline 11.0.1.2 of the Advanced Light Source at Lawrence Berkeley National Laboratory.[39] Films were floated off of poly(styrene)-co-styrene sodium sulfonate (NaPss) deposited glass substrates using deionized water, and then transferred onto 100nm thick SiN2 windows (purchased from Norcada company). Horizontally polarized X-rays at 284.0 eV were aligned normal to the film surface. 284.0 eV was chosen by calculating the scattering materials contrast between PBDTTT-EFT and $PC_{71}BM$.[39] Comparison with non-resonant 270eV photons determined that the low-q component of scattering was from roughness, and not materials contrast. Scattered photons were collected by a Princeton PI-MTE in-vacuum CCD detector with 27.6 um x 27.6 um pixels. Two scattering patterns of 100 sec exposure time were collected at 30 mm and 150 mm sample to detector distances respectively, and combined in software. Two dimensional scattering patterns were reduced to one dimensional profiles by using a customized version of NIKA.[39]

Journal of Materials Chemistry A Accepted Manuscript

This journal is © The Royal Society of Chemistry 20xx

Please do not adjust margins

The absorption spectra of the polymer blend were conducted by a PerkinElmer Lambda 950 UV/VIS/NIR spectrometer.

Results and discussion

Devices were fabricated with an inverted structure of ITO/PEIE/polymer:$PC_{71}BM$/MoO_x/Ag. Polyethylenimine ethoxylated (PEIE) was used as an interfacial layer to lower the work function of ITO, enabling electron collection from the ITO electrode.[40] Compared with the traditional electron transporting metal oxides such as ZnO, PEIE provides an effective way to fabricate devices via solution processing at low temperature, enabling continuous processing on flexible substrates. Conventionally prepared devices were fabricated by spin-coating the active layer from a solution of 1:1.5 PBDTTT-EFT:$PC_{71}BM$ by weight dissolved in 97:3 chlorobenzene:DIO by volume with no anti-solvent treatment. Current density-voltage (J-V) curves measured under simulated AM 1.5G with irradiance of 100 mW/cm^2 are shown in **Fig.2 (a)** with the corresponding photovoltaic parameters of the best performing cells summarized in **Table 1**. The best conventionally prepared device exhibits a short-circuit current density (J_{sc}) of 17.3 mA/cm^2, open circuit voltage (V_{oc}) of 0.80 V and fill factor (FF) of 0.67, yielding a power conversion efficiency of 9.3% with an average value of 9.1%. The external quantum efficiency (EQE) spectra (**Fig.2 (b)**) of organic solar cells based on PBDTTT-EFT covers the range from 350nm to 800nm with the J_{SC} values predicted from integrating EQE spectra (as shown in **Table S1**) showing a good agreement with a discrepancy of less than 10% with the measured short circuit currents under 100 mW/cm^2 AM1.5G. The conventionally prepared device however shows a poor stability, see **Fig.2 (c)-(f)**. **Fig.2 (c)** shows the normalized efficiency of organic solar cells as a function of the ageing time, with device efficiency normalized to their initial value. During the degradation studies, solar cells were stored in ambient atmosphere between testing, subject only to light present in the laboratory (no direct sunlight or prolonged high intensity illumination). The stability test in this study is similar to the protocol ISOS-D-1 shelf and the details of stability test are summarized in **Table S2**.[41] A rapid decrease of efficiency in the conventional device is observed dropping to practically 0% after 30 days of storage. As shown in Fig.**2 (d)-(f)**, the open circuit voltage of the device remains constant, but with a rapid drop in short circuit current and fill factor. An accompanying colour change of the active layer is also observed that starts from the edge of the substrate and progressing into the centre (**Fig.S1**), suggesting that this degradation is linked to oxygen and/or water ingress (devices were simply encapsulated using epoxy and a glass cover slide).

In contrast, the device prepared with the anti-solvent treatment process shows a remarkable improvement in device stability. A number of anti-solvents were tested and the device treated with isopropanol exhibits the best efficiency, see **Fig.S2**. Compared with conventionally prepared device, the performance of the anti-solvent device shows a similar, albeit slightly lower starting efficiency with a J_{SC} of 18.3 mA/cm^2, FF of 0.62, V_{OC} of 0.79 and overall PCE of 9.0 % with an average efficiency of 8.5%. However over same period for which the conventionally prepared device has lost all functionality the anti-solvent treated device retains 80% of its initial efficiency. Similar to the conventionally prepared device, the drop in efficiency for the anti-solvent device is linked to a decrease in J_{SC} and FF with V_{OC} remaining more constant. Although the anti-solvent treated device still shows degradation over this time scale, the combination of this anti-solvent treatment with more effective barrier materials and better encapsulation techniques is a promising route to long term stability.

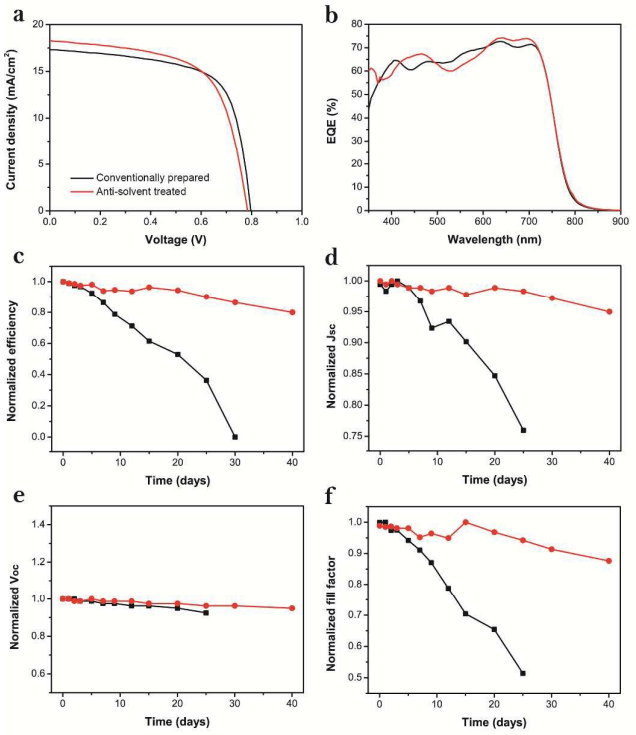

Fig.2 Photovoltaic characterizations of conventionally prepared (black curve) and anti-solvent treated (red curves) blends. (a) current-voltage (J-V) curves of organic solar cells based on PBDTTT-EFT/$PC_{71}BM$ blend, (b) external quantum efficiency (EQE) measurement. (c) normalized power conversion efficiency (PCE), (d) normalized short circuit current (Jsc), (e) normalized open circuit voltage (Voc) and (f) normalized fill factor (FF) as a function of time.

Table 1. Photovoltaic parameters of organic solar cells constructed on PBDTTT-EFT/$PC_{71}BM$ blends.

Device	Voc (V)	Jsc (mA/cm^2)	FF	PCE (%) (average)
Conventionally prepared	0.80	17.3	0.67	9.3% (9.1%)
Anti-solvent treated	0.79	18.3	0.62	9.0% (8.5%)

To further investigate the mechanism behind the degradation of device performance, UV-vis optical absorption spectra were acquired of films (as shown in **Fig.3**) as a function of ageing time (samples were left in ambient under laboratory lighting). Neat PBDTTT-EFT films and neat $PC_{71}BM$ films processed

Journal of Materials Chemistry A Accepted Manuscript

without DIO show good ambient stability under illumination see **Fig.3 (a)** and **(c).** As shown in **Fig.3 (b)**, neat PBDTTT-EFT processed with DIO experiences a systematic increased in absorption strength as a function of time associated with changes in polymer conformation during the slow evaporation of DIO; however no degradation of the neat PBDTTT-EFT processed with DIO is observed over the time frame investigated. Furthermore, the blend of PBDTTT-EFT with $PC_{71}BM$ processed without DIO also shows excellent stability of its UV-vis spectrum (**Fig.3 (d)**). However, the blend processed with DIO exhibits extremely poor stability upon exposure to light and air. After 2 hours of illumination, the colour of film starts to change from the initial dark green to yellow (as shown in **Fig.S3**). The colour of the whole film is observed to change within 6 hours of light illumination under ambient environment. This colour change is spectroscopically confirmed by the UV-Vis absorption spectra shown in **Fig.3 (e)**. The two main absorption peaks located at 710 nm and 645 nm which are attributed to PBDTTT-EFT continuously decrease in intensity with time, indicating the degradation of PBDTTT-EFT with air and light exposure. After 10 hours the UV-vis absorption spectrum of the blend resembles that of neat $PC_{71}BM$ indicating that the optical absorption strength of the polymer has been almost entirely bleached. Degradation of the packing behaviour of polymer is also observed by grazing incident wide angle X-ray scattering (GIWAXS), see **Fig.S4**. The scattering intensity of the in-plane alkyl stacking peak (at q_{xy}=0.30Å) shows a remarkable decrease in intensity after 1 day of air and light exposure as the polymer starts to lose its crystalline structure. In contrast, the blend prepared with the anti-solvent treatment shows very little change in the absorption spectrum, **Fig.3 (f)**.

The observations from the UV-vis experiments are consistent with the following interpretation. 1. $PC_{71}BM$ and PBDTTT-EFT are relatively stable or at least sufficiently stable so as not to degrade over the timescale investigated. 2. Blends of PBDTTT-EFT with $PC_{71}BM$ processed without DIO are similarly stable over the time scale investigated. 3. DIO itself does not render PDBTTT-EFT or $PC_{71}BM$ unstable indicating there is no chemical reaction between DIO and PBDTTT-EFT or DIO and $PC_{71}BM$. 4. The UV-vis absorption spectrum of PBDTTT-EFT processed with DIO, while showing no degradation, does show an evolution in vibronic structure consistent with changes in polymer conformation as DIO slowly evaporates from the film indicating that DIO remains over the time scale of investigation. (In contrast, an anti-solvent treated pristine film shows no evolution in vibronic structure (**Fig.S5**) with the absorption spectrum matching that of a film prepared without DIO indicating that DIO has been removed by the anti-solvent treatment.) The presence of DIO in the film over this timescale is furthermore likely to result in an increased permeability of water and oxygen. 5. The degradation of the blend processed with DIO is explained by the mechanism proposed by Soon et al.[24] whereby singlet oxygen is generated by reaction of triplet excitons on PBDTTT-EFT reacting with molecular oxygen. Such triplet excitons are only formed on PBDTTT-EFT following non-geminate recombination of free carriers that in turn are produced following photo-induced charge transfer thus requiring the presence of $PC_{71}BM$. This reaction also requires the presence of molecular oxygen whose presence in the bulk of the blend is facilitated by residual DIO that increases the permeability of the film to molecular oxygen. Thus the anti-solvent treatment is effective increasing stability of the blend by preventing ingress of oxygen which is required for this somewhat complicated photo-bleaching reaction to occur. The link between residual DIO and device stability is further confirmed by ageing studies of devices prepared without DIO, **Fig.S7**. While such devices have a lower initial efficiency,[5] they exhibit a similar stability to the anti-solvent treated device. The similar stability of the device prepared without DIO also indicates the effectiveness of the anti-solvent treatment in removing DIO from the film.

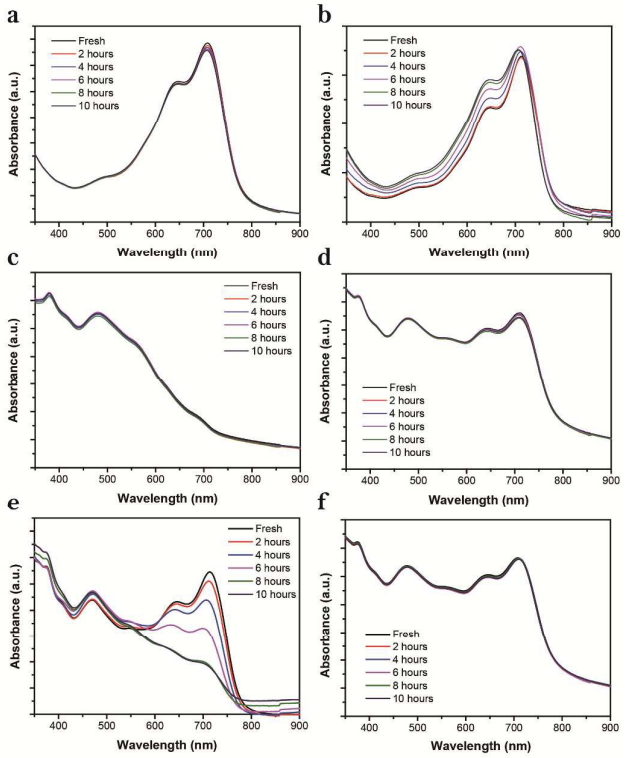

Fig.3 UV-vis spectra as function of ageing time. (a) pristine PBDTTT-EFT processed with DIO, (b) pristine PBDTTT-EFT processed without DIO, (c) pristine $PC_{71}BM$, (d) blend of PBDTTT-EFT/$PC_{71}BM$ processed without DIO, (e) blend of PBDTTT-EFT/$PC_{71}BM$ processed with DIO, and (f) blend of PBDTTT-EFT/$PC_{71}BM$ processed with DIO followed by anti-solvent treatment.

We have also investigated the influence of our anti-solvent treatment on the microstructure of PBDTTT-EFT films with a combination of synchrotron techniques. Two dimensional GIWAXS patterns from conventionally prepared and anti-solvent-treated films are shown in **Fig.4 (a) and (b)**. Both samples were prepared on PEIE coated silicon wafers, matching preparation conditions for devices. In **Fig.4 (a)**, a broad out-of-plane (OOP) peak located at q_z=1.52 $Å^{-1}$ corresponding to polymer π-π stacking is observed while an intense in-plane (IP) peak located at q_{xy}=0.30 $Å^{-1}$ corresponding

Journal of Materials Chemistry A Accepted Manuscript

This journal is © The Royal Society of Chemistry 20xx

Please do not adjust margins

to alkyl stacking or lamellar of the polymer is observed. PBDTTT-EFT in the untreated film shows a preferential face-on configuration with the π-π stacking direction (important for hole transport between polymer chains[42]) perpendicular to the substrate. The distances between crystallographic planes in these directions are calculated by Bragg's law with a π-π stacking distance of 0.41 nm and alkyl stacking distance of 2.09 nm. The isotropic ring at 1.30 $Å^{-1}$ is attributed to the $PC_{71}BM$ aggregation. As shown in **Fig.4 (b)**, the anti-solvent treated blend shows a similar microstructure with a face-on configuration corresponding to a π-π stacking direction perpendicular to the substrate. In addition, no peak position shift is observed in the anti-solvent treated samples, indicating that the molecular packing behaviour is unchanged upon the anti-solvent treatment.

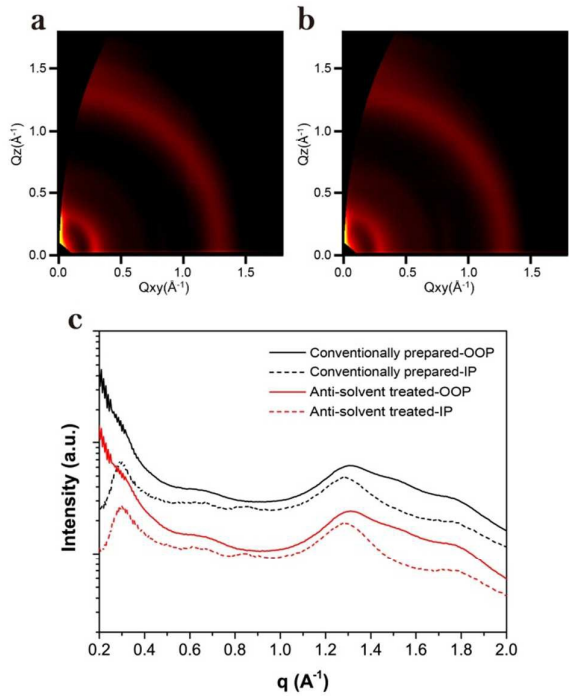

Fig.4 2D GIWAXS scattering patterns of (a) the the conventionally prepared PBDTTT-EFT/$PC_{71}BM$ and (b) the anti-solvent treated PBDTTT-EFT/$PC_{71}BM$. (c) out-of-plane and in-plane line profile for 2D GIWAXS scattering patterns

The full width at half maximum (FWHM) of each peak has been calculated from the corresponding line profiles, with **Fig.4 (c)** showing both of out-of-plane (OOP) and in-plane (IP) scattering profiles. Both of OOP π-π stacking and IP alkyl lamella peaks are fit by Gaussian functions and their FWHMs summarized in **Table S4**. The FWHM of both OOP π-π stacking and IP alkyl lamella peaks does not change appreciably upon the anti-solvent treatment, indicating again that the crystal structure within the film remains unchanged. The anti-solvent treated polymer film shows a slightly lower coherence length of 2.16 nm for OOP π-π stacking and 7.66 nm for IP alkyl stacking compared to values of 2.22 nm (OOP π-π-stacking) and 7.95 nm (IP alkyl stacking).

Complementary to GIWAXS, resonant soft X-ray scattering (R-SoXS) provides information on the size of compositionally similar domains on the 10 nm – 1 μm length scale.[43] R-SoXS results (**Fig.5)** were acquired with a photon energy of 284 eV which provides maximum chemical contrast between polymer and fullerene, see **Fig.S8**. The scattering profiles indicate that PBDTTT-EFT/$PC_{71}BM$ blends with and without anti-solvent treatment have a similar average domain size of around 30nm. This value is close to that observed for other highly efficient polymers such as PTB7 and PffBT4T.[6, 20, 44] AFM has also been performed on conventionally prepared and anti-solvent treated films, see Fig. S9. From the AFM images it is seen that there is an increase in surface roughness even though the bulk domain size remains unchanged.

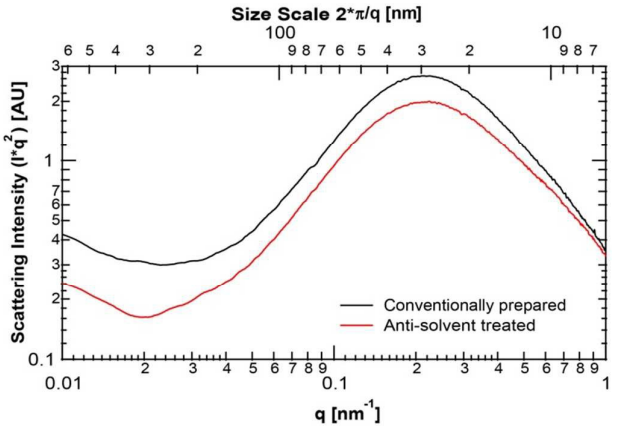

Fig.5 R-SoXS profiles for conventional prepared and anti-solvent treated PBDTTT-EFT/$PC_{71}BM$ blend.

Surface sensitive near edge X-ray absorption fine structure (NEXAFS) spectroscopy has also been employed to provide information about interfacial composition and molecular orientation. Angle-resolved NEXAFS spectra at the surface of the anti-solvent treated blend are shown in **Fig.S10**. The π* resonance intensity in the anti-solvent treated blend film shows a continuous increase as a function of X-ray incident angle, indicating a slight edge-on configuration of the polymer at the polymer/air interface. In addition, **Fig. 6** shows the typical NEXAFS spectra of the pristine polymer film, the pristine fullerene film and the blend film. These NEXAFS spectra were taken at 55˚ to disregard orientational differences.[45] As shown in **Fig.6 (b)**, fitting the blend spectrum to a linear combination of neat spectra (**Fig.6 (a)**) give a polymer surface composition of 62.8% for the conventionally prepared blend and 63.7% for the anti-solvent treated blend. Thus the anti-solvent treatment does not significantly affect the surface composition, with a polymer enrichment at the air/film interface observed in both cases.

It is interesting to compare our results to others who have reported the effects of alcohol treatment on the performance of PTB7:$PC_{71}BM$ devices.[24, 31, 32] In particular previous work has found alcohol treatment leads to improved performance and optimised morphology. In our work, alcohol treatment was not found to improve device performance although device stability

Journal of Materials Chemistry A Accepted Manuscript

was improved. Additionally, we found no change in the characteristic domain size with alcohol treatment. The reason for these different observations is not clear, however we note that our work uses the polymer PBDTTT-EFT which has a different side-chain to PTB7 used in previous studies suggesting that the influence of alcohol treatment is different for different BDT systems. Secondly, the molecular weights used in these different studies are likely to be different, with the potential for alcohol treatment to affect film morphology likely to be molecular weight dependent. Finally, we note that we use a polymeric interlayer instead of a metal oxide interlayer with alcohol treatment likely affecting these interlayers in different ways.

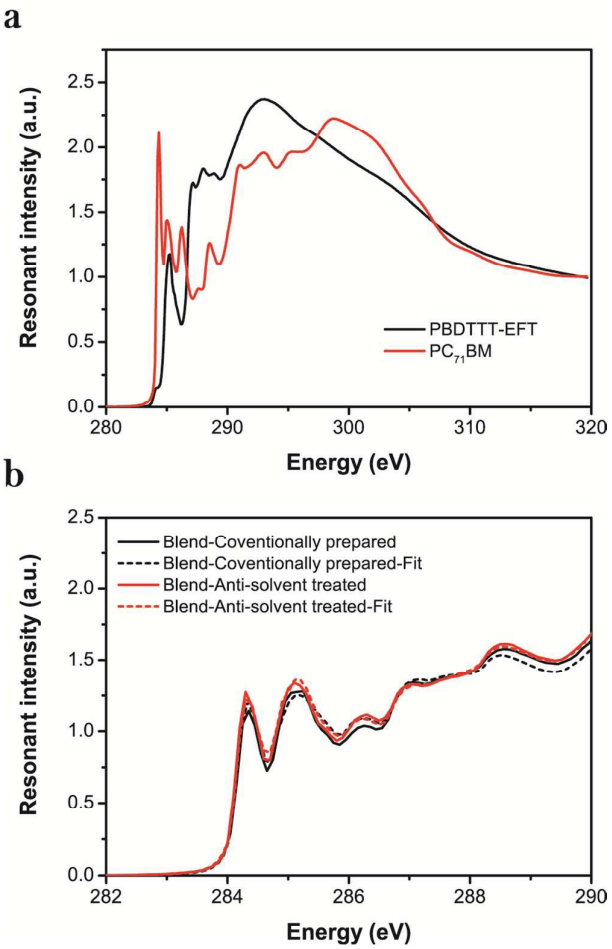

Fig.6 (a) NEXAFS spectra of the pristine PBDTTT-EFT and $PC_{71}BM$ (b) Determination of PBDTTT-EFT:$PC_{71}BM$ volume fraction of conventionally prepared and anti-solvent treated blend. The fit weight fraction of PBDTTT-EFT in the conventionally prepare blend is 62.8% and in the anti-solvent treated blend is 63.7%.

Conclusions

We have reported a simple approach to significantly improve the chemical stability of high efficiency PBDTTT-EFT:$PC_{71}BM$ solar cells. The introduction of an anti-solvent during the spin-coating process induces the fast deposition of the active layer and, importantly, the prompt removal of residual DIO from the film. Removal of the residual DIO inhibits ingress of oxygen suppressing photobleaching leading to a significantly improved device lifetime. Devices prepared with the anti-solvent treatment retain 80% of their initial efficiency over the period that conventionally prepared devices have lost all device function, and also exhibit an initial efficiency close to that of the control device. Microstructural investigations indicate that anti-solvent treated films possess a similar microstructure to conventionally prepared films, with average domain sizes of ~ 30 nm. There is also no significant change in polymer crystallization and chemical composition at the top surface. The simplicity of this process also makes it an industrially-relevant process enabling solvent additives with a low volatility to be used in a high through-put manufacturing environment.

Acknowledgements

NEXAFS spectroscopy and GIWAXS experiments were performed at soft X-ray[35] and SAXS/WAXS[46] beamlines at the Australian Synchrotron, Victoria, Australia. The authors thank Dr. Nigel Kirby for GIWAXS beamline setup. RSoXS experiments were conducted at beamline 11.0.1.2[39] of the Advanced Light Source at Lawrence Berkeley National Laboratory. Support from the Australian Renewable Energy Agency (ARENA) is acknowledged; C.R.M acknowledges support from the Australian Research Council (FT100100275) and veski

Notes and references

1. Z. He, C. Zhong, S. Su, M. Xu, H. Wu and Y. Cao, *Nat. Photonics*, 2012, **6**, 591-595.
2. S.-H. Liao, H.-J. Jhuo, Y.-S. Cheng and S.-A. Chen, *Adv. Mater.*, 2013, **25**, 4766-4771.
3. X. Guo, M. Zhang, W. Ma, L. Ye, S. Zhang, S. Liu, H. Ade, F. Huang and J. Hou, *Adv. Mater.*, 2014, **26**, 4043.
4. T. L. Nguyen, H. Choi, S. J. Ko, M. A. Uddin, B. Walker, S. Yum, J. E. Jeong, M. H. Yun, T. J. Shin, S. Hwang, J. Y. Kim and H. Y. Woo, *Energy Environ. Sci.*, 2014, **7**, 3040-3051.
5. W. Huang, E. Gann, L. Thomsen, C. Dong, Y.-B. Cheng and C. R. McNeill, *Adv. Energy Mater.*, 2015, **5**, 1401259.
6. Y. Liu, J. Zhao, Z. Li, C. Mu, W. Ma, H. Hu, K. Jiang, H. Lin, H. Ade and H. Yan, *Nat. Commun.*, 2014, **5**, 5293.
7. Z. He, B. Xiao, F. Liu, H. Wu, Y. Yang, S. Xiao, C. Wang, T. P. Russell and Y. Cao, *Nat Photon*, 2015, **9**, 174-179.
8. L. Lu and L. Yu, *Adv. Mater.*, 2014, **26**, 4413-4430.
9. L. Ye, S. Zhang, L. Huo, M. Zhang and J. Hou, *Acc. Chem. Res.*, 2014, **47**, 1595-1603.
10. J. You, C.-C. Chen, L. Dou, S. Murase, H.-S. Duan, S. A. Hawks, T. Xu, H. J. Son, L. Yu, G. Li and Y. Yang, *Adv. Mater.*, 2012, **24**, 5267-5272.
11. Y. Liang, Z. Xu, J. Xia, S.-T. Tsai, Y. Wu, G. Li, C. Ray and L. Yu, *Adv. Energy Mater.*, 2010, **22**, E135-E138.
12. S. Guo, J. Ning, V. Körstgens, Y. Yao, E. M. Herzig, S. V. Roth and P. Müller-Buschbaum, *Adv. Energy Mater.*, 2015, **5**, 1401315.
13. C. Cui, W.-Y. Wong and Y. Li, *Energy Environ. Sci.*, 2014, **7**, 2276-2284.

Journal of Materials Chemistry A Accepted Manuscript

This journal is © The Royal Society of Chemistry 20xx

Please do not adjust margins

14. D. Mori, H. Benten, I. Okada, H. Ohkita and S. Ito, *Energy Environ. Sci.*, 2014, **7**, 2939-2943.
15. J. Kong, I.-W. Hwang and K. Lee, *Adv. Mater.*, 2014, **26**, 6275-6283.
16. L. Ye, S. Zhang, W. Zhao, H. Yao and J. Hou, *Chem. Mater.*, 2014, **26**, 3603-3605.
17. M.-S. Su, C.-Y. Kuo, M.-C. Yuan, U. S. Jeng, C.-J. Su and K.-H. Wei, *Adv. Mater.*, 2011, **23**, 3315-3319.
18. J. Peet, J. Y. Kim, N. E. Coates, W. L. Ma, D. Moses, A. J. Heeger and G. C. Bazan, *Nat. Mater.*, 2007, **6**, 497-500.
19. J. K. Lee, W. L. Ma, C. J. Brabec, J. Yuen, J. S. Moon, J. Y. Kim, K. Lee, G. C. Bazan and A. J. Heeger, *J. Am. Chem. Soc.*, 2008, **130**, 3619-3623.
20. B. A. Collins, Z. Li, J. R. Tumbleston, E. Gann, C. R. McNeill and H. Ade, *Adv. Energy Mater.*, 2013, **3**, 65-74.
21. X. Guo, C. Cui, M. Zhang, L. Huo, Y. Huang, J. Hou and Y. Li, *Energy Environ. Sci.*, 2012, **5**, 7943-7949.
22. J. T. Rogers, K. Schmidt, M. F. Toney, E. J. Kramer and G. C. Bazan, *Adv. Mater.*, 2011, **23**, 2284-2288.
23. H. C. Liao, C. C. Ho, C. Y. Chang, M. H. Jao, S. B. Darling and W. F. Su, *Mater. Today*, 2013, **16**, 326-336.
24. L. Ye, Y. Jing, X. Guo, H. Sun, S. Zhang, M. Zhang, L. Huo and J. Hou, *J. Phys. Chem. C*, 2013, **117**, 14920-14928.
25. S. Alem, S. Wakim, J. Lu, G. Robertson, J. Ding and Y. Tao, *ACS Appl. Mater. Inter.*, 2012, **4**, 2993-2998.
26. Y. W. Soon, H. Cho, J. Low, H. Bronstein, I. McCulloch and J. R. Durrant, *Chem. Commun.*, 2013, **49**, 1291-1293.
27. S. Woo, W. Hyun Kim, H. Kim, Y. Yi, H.-K. Lyu and Y. Kim, *Adv. Energy Mater.*, 2014, **4**, 1301692.
28. J. Razzell-Hollis, J. Wade, W. C. Tsoi, Y. Soon, J. Durrant and J.-S. Kim, *J. Mater. Chem. A*, 2014, **2**, 20189-20195.
29. H. Ma, H. L. Yip, F. Huang and A. K. Y. Jen, *Adv. Funct. Mater.*, 2010, **20**, 1371-1388.
30. Z. Xu, L. M. Chen, G. Yang, C. H. Huang, J. Hou, Y. Wu, G. Li, C. S. Hsu and Y. Yang, *Adv. Funct. Mater.*, 2009, **19**, 1227-1234.
31. S. Guo, B. Cao, W. Wang, J.-F. Moulin and P. Müller-Buschbaum, *ACS Appl. Mater. Inter.*, 2015, **7**, 4641-4649.
32. H. Zhou, Y. Zhang, J. Seifter, S. D. Collins, C. Luo, G. C. Bazan, T.-Q. Nguyen and A. J. Heeger, *Adv. Mater.*, 2013, **25**, 1646-1652.
33. N. M. Kirby, S. T. Mudie, A. M. Hawley, D. J. Cookson, H. D. T. Mertens, N. Cowieson and V. Samardzic-Boban, *J. Appl. Crystallogr.*, 2013, **46**, 1670-1680.
34. E. Gann, X. Gao, C.-a. Di and C. R. McNeill, *Adv. Funct. Mater.*, 2014, **24**, 7211-7220.
35. B. C. C. Cowie, A. Tadich and L. Thomsen, *AIP Conf. Proc.*, 2010, **1234**, 307-310.
36. E. Gann, C. R. McNeill, M. Szumilo, H. Sirringhaus, M. Sommer, S. Maniam, S. J. Langford and L. Thomsen, *J. Chem. Phys.*, 2014, **140**, 164710.
37. T. Schuettfort, L. Thomsen and C. R. McNeill, *J. Am. Chem. Soc.*, 2013, **135**, 1092-1101.
38. W. Huang, E. Gann, Y.-B. Cheng and C. R. McNeill, *ACS Appl. Mater. Inter.*, 2015, 14026-14034.
39. E. Gann, A. T. Young, B. A. Collins, H. Yan, J. Nasiatka, H. A. Padmore, H. Ade, A. Hexemer and C. Wang, *Rev. Sci. Instrum.*, 2012, **83**, 045110.
40. Y. Zhou, C. Fuentes-Hernandez, J. Shim, J. Meyer, A. J. Giordano, H. Li, P. Winget, T. Papadopoulos, H. Cheun, J. Kim, M. Fenoll, A. Dindar, W. Haske, E. Najafabadi, T. M. Khan, H. Sojoudi, S. Barlow, S. Graham, J.-L. Brédas, S. R. Marder, A. Kahn and B. Kippelen, *Science*, 2012, **336**, 327-332.
41. M. O. Reese, S. A. Gevorgyan, M. Jørgensen, E. Bundgaard, S. R. Kurtz, D. S. Ginley, D. C. Olson, M. T. Lloyd, P. Morvillo, E. A. Katz, A. Elschner, O. Haillant, T. R. Currier, V. Shrotriya, M. Hermenau, M. Riede, K. R. Kirov, G. Trimmel, T. Rath, O. Inganäs, F. Zhang, M. Andersson, K. Tvingstedt, M. Lira-Cantu, D. Laird, C. McGuiness, S. Gowrisanker, M. Pannone, M. Xiao, J. Hauch, R. Steim, D. M. DeLongchamp, R. Rösch, H. Hoppe, N. Espinosa, A. Urbina, G. Yaman-Uzunoglu, J.-B. Bonekamp, A. J. J. M. van Breemen, C. Girotto, E. Voroshazi and F. C. Krebs, *Sol. Energy Mater. Sol. Cells*, 2011, **95**, 1253-1267.
42. T. M. Clarke and J. R. Durrant, *Chem. Rev.*, 2010, **110**, 6736-6767.
43. C. R. McNeill and H. Ade, *J. Mater. Chem. C*, 2013, **1**, 187-201.
44. S. Guo, E. M. Herzig, A. Naumann, G. Tainter, J. Perlich and P. Müller-Buschbaum, *J. Phys. Chem. B*, 2014, **118**, 344-350.
45. J. Stöhr, *NEXAFS Spectroscopy*, Springer, Berlin, 1992.
46. N. M. Kirby, S. T. Mudie, A. M. Hawley, D. J. Cookson, H. D. T. Mertens, N. Cowieson and V. Samardzic-Boban, *J. Appl. Cryst.*, 2013, **46**, 1670-1680.

Journal of Materials Chemistry A Accepted Manuscript